Catalysis Today 369 (2021) 77–87

Contents lists available at ScienceDirect

Catalysis Today

journal homepage: www.elsevier.com/locate/cattod

Niobium-based solid acids in combination with a methanol synthesis catalyst for the direct production of dimethyl ether from synthesis gas

C. Hernández Mejía, D.M.A. Verbart, K.P. de Jong *

Inorganic Chemistry and Catalysis, Debye Institute for Nanomaterial Science, Utrecht University, Universiteitsweg 99, 3584 CG Utrecht, P.O. Box 80083, 3508 TB Utrecht, the Netherlands

ARTICLE INFO

Keywords:
DME synthesis
synthesis gas
niobium oxide
niobium phosphate
bifunctional catalysis

ABSTRACT

The production of dimethyl ether (DME) as compared to methanol from synthesis gas allows for increased conversions in a single pass. A challenge in this process is the combination of methanol synthesis and dehydration functionalities in a single catalyst without mutual negative interference of their performances. Here, we studied the use of hydrated niobium pentoxide ($Nb_2O_5{\cdot}nH_2O$) and niobium phosphate ($NbOPO_4$) in combination with a copper-based methanol synthesis catalyst in the direct synthesis of DME, while gamma-alumina (γ-Al_2O_3) was used as a reference material. The three solid acids combined with the copper-based catalyst proved active and selective in the production of DME, however all of them showed some degree of deactivation throughout the reaction. Characterization of the used catalysts pointed out that while the γ-Al_2O_3-based mixture deactivated most likely due to coke deposition on the alumina and structural changes in the methanol synthesis catalysts, the $Nb_2O_5{\cdot}nH_2O$ and $NbOPO_4$-based catalysts lost activity probably as a result of copper migration from the methanol synthesis catalyst to the acid component. In view of the high volume-based activity of the Nb-based solid acids it is concluded that these are promising components for the direct catalytic conversion of synthesis gas to DME.

1. Introduction

Synthesis gas, a mixture of hydrogen and carbon monoxide, is a versatile feedstock for the production of various chemicals and fuels. The conversion of synthesis gas to a desired product relies substantially on the catalyst employed. Whereas a primary hydrogenation function, typically a late-transition metal, can selectively produce chemicals such as alcohols, olefins or paraffins, addition of a second catalyst can be employed to couple reactions and expand the diversity of products[1,2]. Ideally, both functionalities in a catalyst mixture should result solely in a positive synergetic performance, which is feasible by selecting the appropriate chemical properties and an optimal degree of intimacy [3–6]. However, achieving the ideal composition without negative interferences remains a challenge in these multifunctional catalytic systems.

Dimethyl ether (DME) is commonly utilized in the aerosol industry as propellant and in the chemical industry as methylating agent, and it has shown potential in the production of bulk chemicals such as olefins, aromatics and acetic acid[7–11]. Moreover, DME has attracted interest during the last decades as a clean fuel owing to its similar physicochemical properties to LPG and low particulate emissions [12–16]. DME can be directly produced by coupling the synthesis of methanol from synthesis gas with the dehydration of methanol to DME. Haldor Topsøe initially recognized the industrial advantages of combining both reactions in a single process, showing that the direct production of DME from synthesis gas could improve energy efficiencies and reduce capital costs[14,15,17]. Fig. 1 shows the relevant reaction equations for the synthesis of DME and their corresponding thermodynamic equilibria. While methanol formation from synthesis gas is an equilibrium-limited reaction (Fig. 1, eq. 1), in-situ conversion of methanol towards DME shifts this equilibrium towards higher conversions in a single pass, a benefit of combining both reactions (Fig. 1, eq. 2 and 5). The additional water formed during the dehydration can bring about the water-gas-shift reaction, in which H_2O and CO react to form CO_2 and H_2 (Fig. 1, eq. 3). This can be beneficial when using hydrogen-deficient synthesis gas but also the presence of CO_2 can enhance the synthesis of methanol[18] (Fig. 1, eq. 4). However, an excess of water can further boost the water-gas-shift reaction at the expense of methanol synthesis decreasing the DME yield of the catalyst[19]. Water can also lead to detrimental effects on the catalysts' structure, such as sintering or

* Corresponding author.
E-mail address: k.p.dejong@uu.nl (K.P. de Jong).

https://doi.org/10.1016/j.cattod.2020.07.059
Received 28 October 2019; Received in revised form 11 June 2020; Accepted 13 July 2020
Available online 28 July 2020

poisoning of active sites, resulting in an accelerated deactivation[19,20]. The direct synthesis of DME from synthesis gas is therefore a clear example of the advantages and challenges in bifunctional catalysis[21,22].

Currently, the most efficient methanol synthesis catalysts are copper-based and hence widely used in industry[23]. Methanol synthesis is an exothermic reaction and it is accompanied with a volumetric contraction, the preferred reaction conditions are therefore low temperatures and high pressures according to Le Chatelier's principle (Fig. 1, eq. 1). Thus, methanol synthesis catalysts are typically operated at pressures between 30 – 50 bar and temperatures in the range of 220 – 300 °C, such conditions result in methanol selectivity greater than 99 % and reduced formation of by-products[24,25]. Furthermore, it is well known that methanol can be synthetized from CO_2-enriched synthesis gas (Fig. 1, eq. 4), making it a target for research on CO_2 utilization[26,27]. Methanol dehydration to form DME (Fig. 1, eq. 2) is also an exothermic process and can be performed at relatively low temperatures (150 – 300 °C). Thus, the similarity of the process conditions makes it possible to operate methanol synthesis and DME production in a single reactor. The synergy generated by introducing the methanol dehydration reaction leads to a significant increase in CO conversion per pass (Fig. 1, eq 5), this is in marked contrast to the two-step process in which methanol is produced separately, stored and further converted to DME. The resulting equilibrium composition as a function of temperature for the direct DME synthesis is shown in Fig. 2, when considering the presence of CO, H_2, methanol, DME, CO_2 and H_2O at 40 bar total pressure. It is possible to observe that DME is favored as the main product at temperatures below 300 °C, and the other molecules can be recycled to produce more DME.

Methanol dehydration can be catalyzed by Brønsted as well as Lewis acid sites and the most studied solid acids for this reaction are γ-Al_2O_3 and zeolites[21,22,28,29]. Too strong acid sites and high temperatures can favor the further dehydration of DME to olefins and hydrocarbons [30], compromising the selectivity of the catalyst. This is the case for most zeolites, which contain strong acid sites favoring DME dehydration at the required temperatures for methanol synthesis[31]. Even though various strategies exist to tune the zeolites' acidity[32,33], their microporous structure can restrain the diffusion of methanol, DME and hydrocarbons leading to further polymerization reactions and coke formation, inactivating and blocking the active sites[34]. γ-Al_2O_3 on the other hand, possesses milder acid sites, mainly of the Lewis type, making it more selective for DME and used for industrial catalysts[14,35,36]. Nonetheless, competitive adsorption of water as well as crystal phase transformation aided by steam make γ-Al_2O_3 sensitive to the formed water during dehydration and thus diminishes its catalytic activity[35,

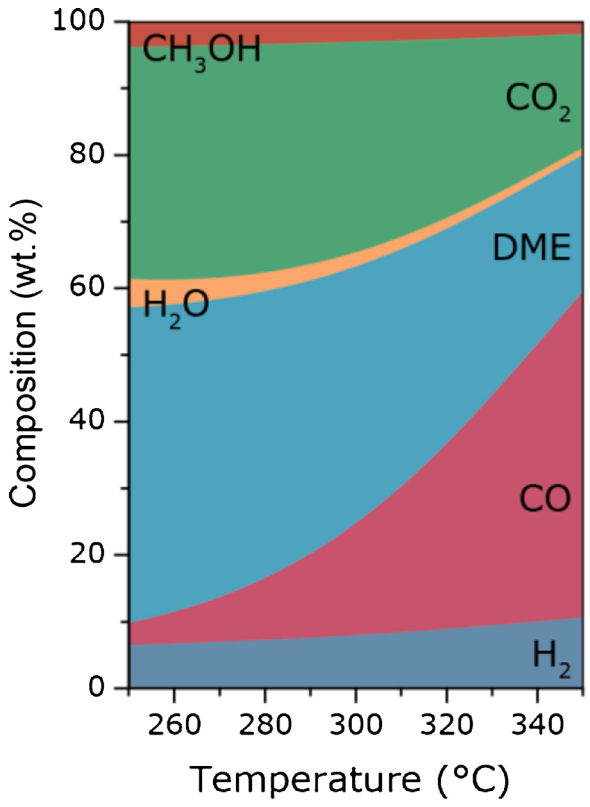

Fig. 2. Equilibrium composition of species involved in the direct synthesis of DME as a function of temperature at 40 bar. The thermodynamic calculation was carried out considering all species in the gas phase, a synthesis gas composition of H_2:CO = 2 v/v and DME, methanol, water and CO_2 as possible species. The HSC software from Outotec (v 7.14) was used to perform the calculation.

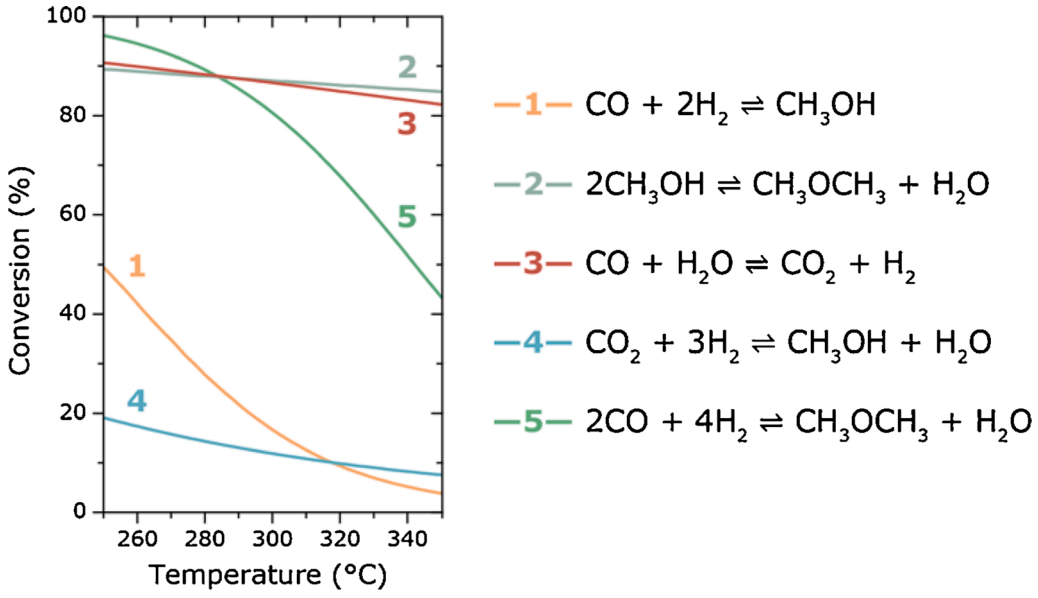

Fig. 1. Thermodynamic equilibrium for stoichiometric quantities of reactants for the individual reactions involved in the synthesis of DME. Calculations were performed using the HSC software from Outotec, v 7.14 in the temperature range from 250 – 350 °C, considering all species in the gas phase and 40 bar total pressure. Conversion refers to that of CO (eq. 1, 3 and 5), CO_2 (eq. 4) or methanol (eq. 2).

37,38].

Hydrated niobium pentoxide ($Nb_2O_5{\cdot}nH_2O$) and niobium phosphate ($NbOPO_4$) are interesting solid acids, possessing both Brønsted and Lewis acid sites, which have shown exceptional catalytic performance for various acid-catalyzed reactions[39–41]. Contrary to many solid acids, these materials are capable of maintaining high catalytic activity and stability when water is involved. This resistance to water poisoning has been reported to originate from Lewis acid sites, in this case coordinatively unsaturated Nb^{5+} cations in NbO_4 tetrahedral arrangements, capable of forming active NbO_4-H_2O adducts that preserve an effective positive charge[42–44]. Thus, niobium-based materials have raised the research interest as stable solid acids for hydration and dehydration reactions. Several studies have reported the application of niobium-based and niobium-modified materials for the dehydration of methanol to form DME[45–47] and for the direct synthesis of DME from synthesis gas[48,49]. These studies have shown the potential of niobium-based materials as active and selective catalysts for the synthesis of DME, however little attention has been paid to their stability.

In this research we studied the catalytic performance of $Nb_2O_5{\cdot}nH_2O$ and $NbOPO_4$ acting as solid acids in concert with a Cu-based catalyst in the direct synthesis of DME from synthesis gas. Particularly, this research focused on the stability of such materials under industrially relevant conditions (40 bar total pressure and 260 or 280 °C) up to 120 h on stream. For this end, we worked with physical mixtures composed of a commercial methanol synthesis catalyst and a solid acid, $Nb_2O_5{\cdot}nH_2O$, $NbOPO_4$ or γ-Al_2O_3, which was used as reference material. The mixtures of the niobium-based solid acids showed comparable activity and DME selectivity than the gamma-alumina one, while all catalysts showed deactivation throughout the reaction. Characterization of the used materials indicated that migration of copper from the methanol synthesis catalyst to the niobium-based materials contributed to the loss in methanol and DME production, whereas in the case of the gamma-alumina mixtures, coke deposition on the alumina and structural alteration of the copper-based catalyst were the main causes of deactivation.

2. Experimental

2.1. Materials

Hydrated niobium pentoxide ($Nb_2O_5{\cdot}nH_2O$, HY-340) and niobium phosphate ($NbOPO_4$) were provided by Companhia Brasileira de Metalurgia e Mineração (CBMM). The gamma-alumina (γ-Al_2O_3) was obtained from BASF as extrudates (Al-3992E1/8"), which were grinded and sieved after thermal treatment. Thermal treatment of the solid acids was performed in stagnant air at different temperatures in all cases for 4 h with a ramp of 5 °C min^{-1}. Thereafter, the materials were sieved in a 38–75 μm fraction. The methanol synthesis catalyst employed was obtained from Alfa Aesar (I06Z036), with a reported composition of 10.1% Al_2O_3, 63.5% CuO, 24.7% ZnO and 1.3% MgO. The catalyst pellets were grinded and sieved in a 75 - 150 μm fraction.

The bulk density of the sieved solid acids and methanol synthesis catalyst was determined by using a 200 μL spoon. The corresponding mass was measured by weighting the volume of material obtained with the spoon. This was repeated for five times and the average of weights was used to calculate the density (Table 1).

The physical mixtures for the direct synthesis of DME were prepared by weighting the desired amount of methanol synthesis catalyst and solid acid, mixed with ~200 mg of SiC (212–425 μm) and loaded in the reactor. For the experiment in stacked-bed configuration, an amount of solid acid fixed to have the same amount of acid sites per reactor ($6{\cdot}10^{-3}$ $mmol_{NH3}$ at 260 °C and $3{\cdot}10^{-3}$ $mmol_{NH3}$ at 280 °C from ammonia TPD) was mixed with ~ 60 mg SiC (212–425 μm) and placed downstream of the methanol synthesis catalyst with ~ 40 mg of SiC (212–425 μm) separating both catalysts beds. Around 20 mg of copper-based methanol synthesis catalyst were used for the experiments at 260 °C and around 10 mg for the experiments at 280 °C, diluted with ~60 mg of SiC (212–425 μm).

2.2. Characterization

Powder X-ray diffractograms of passivated samples were measured using a Bruker-AXS D2 Phaser X-ray diffractometer, Co-Kα radiation (λ =1.7903 Å) with a 1.0 mm fixed slit. Reduced Cu-based methanol synthesis catalyst (25 vol% H_2/N_2 flow, 2 h at 250 °C, heating rate of 5 °C min^{-1}) was placed in an air-tight sample holder and diffraction patterns were recorded on a Bruker D8 advance, equipped with a variable slit and Co-Kα radiation (λ =1.7903 Å). Patterns were compared with the PDF-4+-database. Cu crystallite size was calculated using the Scherrer equation (k = 0.94) to the (111) diffraction line at 2θ = 50.7°, with the Fityk 1.3.1 software[50].

A micromeritics TriStar 3000 apparatus was used to perform N_2-physisorption at −196 °C. Prior to analysis the samples were dried at 200 °C for 16 h in N_2 flow. Specific surface area was calculated using the BET theory for $p/p_0 = 0.06 - 0.25$. The pore size distribution was determined using the BJH theory applied to the adsorption branch. The specific mesopore volume was calculated using single point at $p/p_0 = 0.98$.

Thermogravimetric measurements were performed using a Perkin Elmer TGA8000, hyphenated with a Hiden HPR-20 mass spectrometer. The experiments took place under an oxidizing flow composed of 20 vol. % O_2/Ar. First, the temperature of the sample was held at 30 °C for 5 min. and thereafter heated to 800 °C at 10 °C min^{-1}. The mass spectrometer was used to monitor carbon dioxide (m/z = 44) and water (m/z = 18) throughout the experiment.

Ammonia temperature programmed desorption (NH_3-TPD) analyses were performed using a Micromeritics AutoChem 2990 instrument equipped with a TCD detector. Typically, 100 mg of sample were dried in a He flow at the corresponding calcination temperature for each sample. The samples were then cooled to 100 °C in a He flow, followed by pulses of 10 vol% NH_3/He until saturation was reached. The temperature (100 °C) and He flow were maintained for 1 h. Thereafter, the sample was heated under He flow to 400 °C ($Nb_2O_5{\cdot}nH_2O$ and $NbOPO_4$) or 600 °C (γ-Al_2O_3) at a rate of 10 °C min^{-1}, the desorption of ammonia was monitored by the TCD detector. NH_3-TPD profiles can be found in Fig. S1.

FTIR spectroscopy of adsorbed pyridine was carried out using a Bruker Vertex 70v spectrometer. Each sample was pressed into a self-supporting wafer (diameter 13 mm) and placed in an environmental

Table 1
Summary of the properties of the solid acids.

Solid Acid	Bulk density	Specific Surface Area[a]	NH_3 uptake [b]		Acid sites surface concentration	Lewis/Brønsted acid sites ratio [c]	
	($g{\cdot}mL^{-1}$)	($m^2{\cdot}g^{-1}$)	($mmol_{NH3}{\cdot}g^{-1}$)	($mmol_{NH3}{\cdot}mL^{-1}$)	($mmol_{NH3}{\cdot}m^{-2}$)	Pre-treated at 300 °C	Pre-treated at 400 °C
$Nb_2O_5{\cdot}nH_2O$	0.78	92	0.31	0.24	0.0034	0.9	1.4
$NbOPO_4$	0.90	238	0.60	0.54	0.0025	0.5	0.7
γ-Al_2O_3	0.53	190	0.62	0.33	0.0033	-	-

[a]Determined by N2-physisorption.
[b]Determined by NH3-TPD after pretreatment at 400 °C for Nb2O5·nH2O and NbOPO4 and at 600 °C for γ-Al2O3.
[c]Determined by FT-IR with pyridine as probe molecule.

transmittance IR cell. Samples were first pre-treated under dynamic vacuum (~10^{-6}mbar) at their corresponding calcination temperature (300, 400 or 500 °C, 10 °C min^{-1}), thereafter the sample was cooled down to room temperature and exposed to an excess of pyridine. Then, dynamic vacuum (~10^{-6}mbar) was applied to the sample and heated to 150 °C for 1 h. Spectra were recorded in the 4000 – 1000 cm^{-1} range. The quantitative determination of Lewis and Brønsted acid sites was made using the bands at 1448 and 1540 cm^{-1} following the procedure reported in ref [51].

Scanning transmission electron microscopy (STEM) images were acquired with a FEI Talos F200X microscope operated at 200 kV equipped with 4 energy dispersive X-ray (EDX) detectors, a high-angle annular dark-field (HAADF) and a bright field detector. Samples were prepared by dipping the Au sample grid into the used catalyst.

2.3. Catalytic performance

The catalytic performance was evaluated using an Avantium Flowrence 16 parallel, continuous flow, fixed bed reactor system. The catalysts were reduced *in-situ* at atmospheric pressure in a 25 vol% H_2/He flow, for 2 h at 250 °C (heating rate of 5 °C min^{-1}), this in order to activate the methanol synthesis catalyst by reducing the copper oxide to metallic copper. Thereafter, the gas stream was switched to H_2/CO = 2.0 v/v, with different GHSV depending on the catalyst. Reactors were slowly pressurized by increasing the pressure by 10 bar increments and waiting for 5 min to equilibrate until reaching 40 bar, subsequently reactors were heated to reaction temperature 260 or 280 °C (1 °C min^{-1}). A reactor containing only SiC (200 mg) was used as blank experiment. Products were analyzed using an on-line three-channel gas chromatograph (GC, Agilent 7890B). Hydrogen, carbon monoxide, helium, nitrogen and carbon dioxide were separated on a MolSieve 5A column (2.4 m, 1/8 inch inner diameter) and quantified using a thermal conductivity detector. Methanol, dimethyl ether and C_1-C_4 hydrocarbons were separated using a GS-GasPro column (GS-Gaspro 30 m x0.32 mm ID) and a HP-Innowax column (6 m, 0.32 mm ID) and analyzed by flame ionization detectors. The integrated peak areas were used to determine the gas phase composition, with He as the internal standard. Selectivities reported here were based on carbon atoms ($\%_C$) within hydrocarbons formed. In some experiments selectivities did not add up to 100 % because of tailing of the methanol peak in the chromatogram and some unidentified compounds (likely oxygenates). Gas-Hourly-Space-Velocities (GHSV) were defined as total gas flow divided by the total catalyst volume (not considering the SiC volume). Thermodynamic equilibrium calculations were carried out with the HSC software from Outotec (v 7.14), at 260 °C or 280 °C, considering all species in the gas phase (40 bar total pressure), a synthesis gas composition of H_2:CO = 2 v/v and DME, methanol, water and CO_2 as possible species.

3. Results and discussion

3.1. Structural, textural and acidic properties of the solid acids

$Nb_2O_5{\cdot}nH_2O$ and $NbOPO_4$ are known to have various crystal structures and metastable polymorphs depending on the thermal treatment to which they have been exposed[52,53]. In general, crystallization in these materials occurs around 500 °C for $Nb_2O_5{\cdot}nH_2O$ and 800 °C for $NbOPO_4$, when treated below these temperatures both remain amorphous[41,54,55]. Powder X-ray diffraction (XRD) patterns in figure S2 show that effectively after calcination at 200 or 400 °C for $Nb_2O_5{\cdot}nH_2O$ and 200, 400 or 600 °C for $NbOPO_4$, both materials did not show sharp diffraction signals but broad scattered diffraction patterns characteristic of a largely amorphous structure. Higher calcination temperatures induced crystallization. An increase of the temperature treatment is also accompanied by a loss in specific surface area as previously reported for niobium pentoxide[55,56]. This was the same case for niobium phosphate as shown by the results obtained from N_2-physisorption for samples calcined at different temperatures (Fig. S3). Previous reports have shown that the decrease of surface area occurs together with a decrease of the concentration and strength of acid sites, particularly when reaching crystallization [43,54,57]. Therefore, in order to maintain the acidic properties of both materials and considering the optimal reaction temperature for the direct synthesis of DME (250 - 300 °C), a calcination temperature of 400 °C (4 h, 5 °C min^{-1}) was selected as pre-treatment for both materials. γ-Al_2O_3 was calcined at 600 °C to ensure the gamma phase (Fig. S2, C). Table 1 summarizes the N_2-physisorption, NH_3-Temperature Programmed Desorption (NH_3-TPD) and FT-IR with pyridine as probe molecule characterization results for $Nb_2O_5{\cdot}nH_2O$, $NbOPO_4$ and γ-Al_2O_3.

The interaction of pyridine with the surface of the solid acids was used to assess the nature of such acid sites. The FT-IR spectra region between 1700 – 1400 cm^{-1} shows the vibrations of pyridine interacting with a solid acid[58–61] and employed to determine the ratio of Lewis and Brønsted acid sites (Table 1). The corresponding spectra are shown in Fig. S4, in which IR bands can be observed at ~1446 and 1606 cm^{-1} corresponding to pyridine coordinated to Lewis acid sites (highlighted in green), whereas IR bands corresponding to pyridinium ion on Brønsted acid sites are observed at ~ 1639 and 1540 cm^{-1} (highlighted in red). Additionally, a common IR band for both sites is observed at 1489 cm^{-1} (highlighted in yellow). $Nb_2O_5{\cdot}nH_2O$ and $NbOPO_4$ show bands corresponding to both Lewis and Brønsted acid sites, however $NbOPO_4$ compared to $Nb_2O_5{\cdot}nH_2O$ shows more intense bands at ~1639 and 1540 cm^{-1} (more pyridinium ion on Brønsted acid sites) and a lower ratio of Lewis to Brønsted acid sites. The γ-Al_2O_3 sample displayed only bands at ~1446 and 1606 cm^{-1} and not at ~1639 and 1540 cm^{-1}, an indication that mainly Lewis acid sites are present on the surface of the alumina and no strong Brønsted acid sites to form pyridinium ions. Spectra for $Nb_2O_5{\cdot}nH_2O$ and $NbOPO_4$ pretreated at 300 °C are also included in Fig. S4. For both materials it can be observed that an increment of the pre-treatment temperature from 300 to 400 °C increased the relative intensity of the band at ~1446 cm^{-1} and decreased the one at ~1540 cm^{-1}, therefore the Lewis to Brønsted acid sites ratio increased which is consistent with previous reports[54,56,62]. The increase in Lewis acid sites has been ascribed to removal of surface water by the heat treatment, exposing more Lewis acid sites [54]. This shows that the two niobium-based solid acids presented both Lewis and Brønsted acid sites, $NbOPO_4$ with more Brønsted acid sites compared to $Nb_2O_5{\cdot}nH_2O$, while γ-Al_2O_3 showed mainly Lewis acid sites. Both types of acids can catalyze the dehydration of methanol, however differences in their catalytic performance can be expected due to their distinct mechanisms for DME formation[63–65]. Moreover, due to the high steam pressures during DME synthesis, it is likely that the in-situ generation of Brønsted acid sites affects the performance of the solid acids.

3.2. Catalytic performance

The catalytic performance of the three solid acids was evaluated by preparing physical mixtures with a copper-based methanol synthesis catalyst. These physical mixtures were made by mechanically mixing the 20 mg of copper-based methanol synthesis catalyst (sieve fraction 75 - 150 μm) and ~ 0.2 mL of the solid acid (sieve fraction 38 - 75 μm), 1:13 v/v Cu-based catalyst to solid acid. Therefore, each reactor contained similar volumes of catalyst and hence similar Gas-Hourly-Space-Velocities (GHSV). A summary of the exact compositions and the corresponding results of the catalytic performance for all physical mixtures can be found in Table 2.

DME synthesis was carried out with an H_2 to CO ratio of 2, at 40 bar and for 120 h. The performance was evaluated at 260 or 280 °C, since it has been reported[66] that water poisoning on γ-Al_2O_3 was avoided by raising the reaction temperature above 270 °C. A reaction temperature of 280 °C might then diminish the detrimental effects of water on the solid acids. The physical mixtures in all cases triple the CO conversion for both temperatures compared to the Cu-based catalyst only (Fig. 3 A

Table 2
Summary of the reactor content and catalytic performance results for the physical mixtures and methanol synthesis catalyst only. Reaction conditions: 40 bar, $H_2/CO = 2$ v/v, GHSV (physical mixtures) =1050 h^{-1}, GHSV (methanol synthesis catalyst) =15000 h^{-1}, 260 or 280 °C and TOS =120 h. The values in parenthesis indicate selectivity and yield values excluding CO_2.

Reactor content						Catalytic performance						
Reaction Temperature (°C)	Solid Acid	Mass of Methanol Synthesis Catalyst (g)	Mass of Solid Acid (g)	Total Volume (mL)	Total Amount acid sites[a] ($mmol_{NH3}$)	CO Conversion (%)	DME Productivity ($g_{DME} \cdot h^{-1} \cdot mL^{-1}$)	DME Yield (%C)	DME Selectivity (%C)	MeOH Selectivity (%C)	CO_2 Selectivity (%C)	C_1-C_4 Hydrocarbon selectivity (%C)
	Physical Mixtures											
	$Nb_2O_5 \cdot nH_2O$	0.021	0.152	0.21	0.0047	62	0.26	34 (43)	55 (69)	12 (15)	20	3 (4)
260	$NbOPO_4$	0.020	0.178	0.23	0.0107	53	0.26	35 (46)	66 (87)	6 (8)	24	1 (1)
	γ-Al_2O_3	0.021	0.108	0.21	0.0067	44	0.21	29 (39)	66 (89)	5 (6)	26	1 (1)
	$Nb_2O_5 \cdot nH_2O$	0.020	0.161	0.22	0.0050	75	0.37	49 (63)	65 (84)	5 (7)	23	5 (7)
280	$NbOPO_4$	0.020	0.181	0.23	0.0109	73	0.37	49 (64)	66 (88)	4 (5)	25	2 (3)
	γ-Al_2O_3	0.020	0.105	0.21	0.0065	69	0.34	45 (60)	66 (87)	4 (5)	24	2 (3)
	Methanol synthesis catalyst											
260	–	0.020	–	0.015	–	16	-	0.0	0.0	99.1		0.9
280	–	0.020	–	0.015	–	25	-	0.0	0.0	98.6		1.4

[a]Determined by NH_3-TPD.

and B). This increase in conversion by the addition of the solid acid to the copper-based catalyst originates by two effects: first, the conversion of methanol to form DME shifts the equilibrium to higher CO conversions and second, water formed from the DME synthesis enables the water-gas-shift reaction, producing CO_2 (observed as one of the products) which accelerates methanol production as shown in Fig. 1. The change in CO conversion throughout the experiment was different for each solid acid as shown in Fig. 3 A and B. Despite a similar initial CO conversion within catalysts at 260 °C, the γ-Al_2O_3 mixture lost ~40 % of the conversion after 120 h on stream whereas the $NbOPO_4$ mixture lost ~30 % and the $Nb_2O_5 \cdot nH_2O$ mixture ~15 %. At 280 °C, and higher initial CO conversions, the activity loss was less pronounced but following a similar trend.

Addition of any of the solid acids to the methanol synthesis catalyst effectively changed the selectivity from almost exclusively methanol to mainly DME (Table 2). Particularly $NbOPO_4$ and γ-Al_2O_3 showed the highest DME selectivities, the rest of the products consisted of methanol, CO_2 and a small fraction of C_1-C_4 hydrocarbons, mainly CH_4 and C_2H_6 and in a lesser amount C_2H_4, C_3H_6, C_3H_8, C_4H_8 and C_4H_{10}. Fig. 4 presents the DME, methanol, CO_2 and hydrocarbons selectivities for the physical mixtures throughout the experiment at 260 °C and 280 °C, 40 bar and $H_2/CO = 2$ v/v. At 260 °C, all physical mixtures showed a decrease in DME selectivity throughout the experiment, as well for the CO_2 selectivity. Methanol selectivity during the experiment increased slightly for the niobium-based solid acids, while for the γ-Al_2O_3 catalyst had a minimum decrease. An increase of methanol together with a decrease of DME points to an activity increasingly controlled by the methanol dehydration reaction in particular for the niobium-based catalysts, while a decrease of both methanol and of DME selectivities of the γ-Al_2O_3 catalyst suggests an activity controlled by the methanol synthesis reaction.

An increase of the reaction temperature from 260 to 280 °C increased the activity in all cases but also in the case of $Nb_2O_5 \cdot nH_2O$ improved the DME selectivity while decreasing the methanol selectivity. An increase in methanol dehydration activity to DME in this temperature range has been previously observed for $Nb_2O_5 \cdot nH_2O$[45], which is also observed in this study. For the $NbOPO_4$ and γ-Al_2O_3 catalysts, the increase in reaction temperature had a minimum effect in their selectivities. Volume-based DME productivity was higher for the physical mixtures containing niobium-based acids compared to the γ-Al_2O_3--based mixtures, due to the high density of the niobium materials. Furthermore, the mixtures with $Nb_2O_5 \cdot nH_2O$ and $NbOPO_4$ also showed a higher yield towards DME.

The relative change in DME yield through time is shown in Fig. 5 for the different physical mixtures. $NbOPO_4$ and γ-Al_2O_3 showed similar trends in relative DME yield, losing ~ 30 % at 260 °C and ~ 15 % at 280 °C, while $Nb_2O_5 \cdot nH_2O$ lost ~ 15 % at 260 °C and ~ 10 % at 280 °C. In Table 2, selectivities reported in parenthesis exclude CO_2 since in an industrial process it can be recycled with the unconverted synthesis gas to form more DME. Considering this, DME selectivities can increase in a single pass to ~90 %. On the other hand, the formation of hydrocarbons constitutes a loss of available carbon to further form methanol or DME and thus undesired in this process.

Hydrocarbon formation constitutes an undesired side reaction in methanol and DME synthesis, thus relevant to discuss. The change in hydrocarbons selectivity through time is shown in Fig. 4D and H for the different physical mixtures, in all cases a slight increase in the selectivity to hydrocarbons was observed during the experiment. At a reaction temperature of 260 °C (Fig. 4D), the mixtures containing $NbOPO_4$ and γ-Al_2O_3 had similar selectivities as the methanol synthesis catalyst throughout the experiment (~1 %C), an indication that these products might have mainly originated from the copper-based catalyst under these conditions. The $Nb_2O_5 \cdot nH_2O$-based mixture however showed an increased hydrocarbon selectivity compared to the other catalysts, particularly at the first hours of the experiment. An increase of the reaction temperature to 280 °C increased also the selectivity to

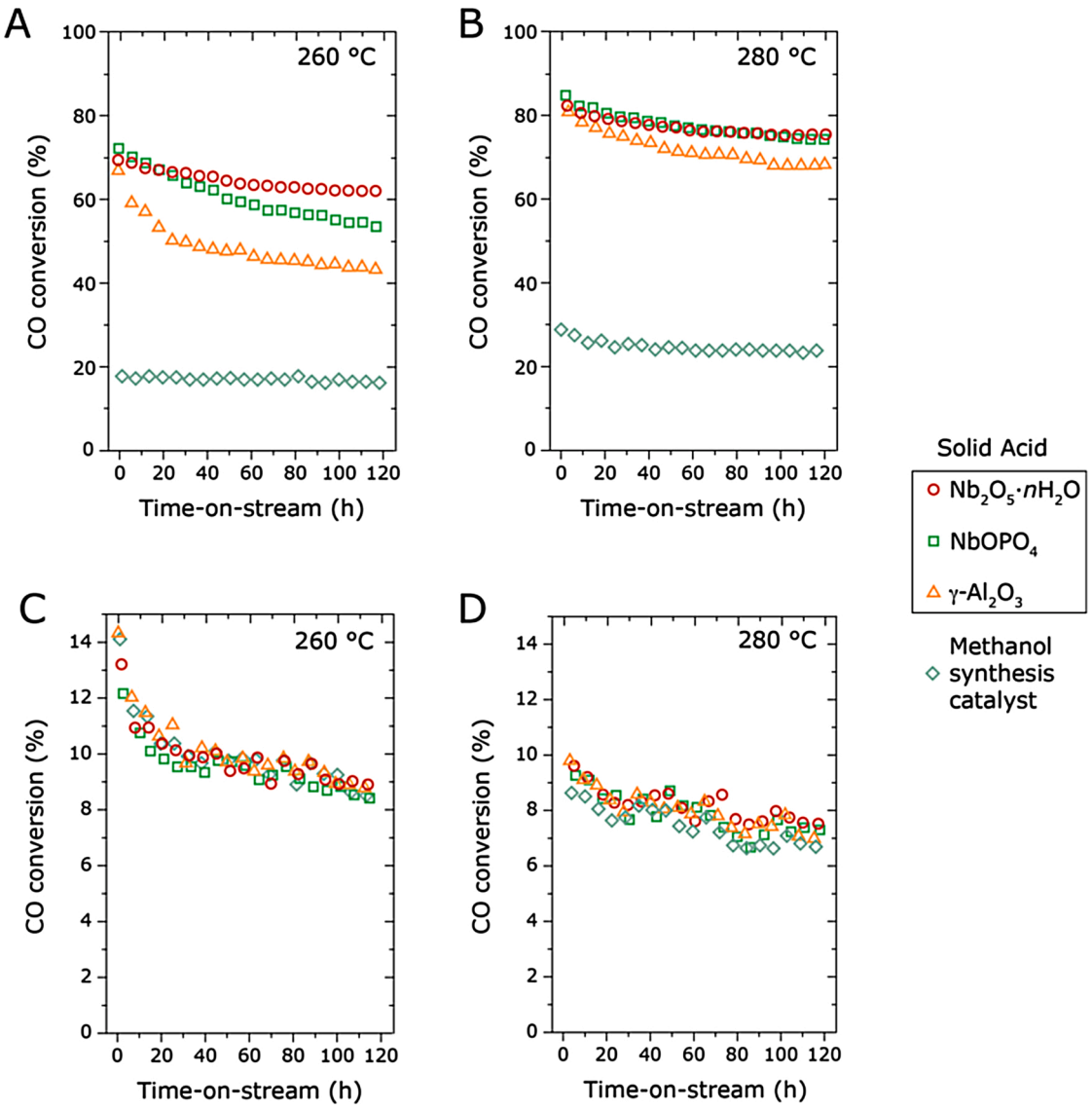

Fig. 3. CO conversion as a function of time-on-stream for the physical mixtures (A and B) and the catalysts in stacked-bed configuration with the solid acid downstream of the methanol synthesis catalyst (C and D) at 260 °C (A and C) or 280 °C (B and D). The performance of the methanol synthesis catalyst only is also shown (grey diamonds). Reaction conditions: 40 bar, $H_2/CO = 2$ v/v. Under these reaction conditions the thermodynamic equilibrium CO conversion to DME is 94 % at 260 °C and 89 % at 280 °C, for methanol synthesis is 40 % at 260 °C and 27 % at 280 °C.

hydrocarbons for all catalysts (Fig. 4H), although in different proportion for each of them. The methanol synthesis catalysts showed a constant selectivity after 20 h on stream resulting in 1.4 $\%_C$ hydrocarbons at the end of the experiment, 0.5 % more than at a reaction temperature of 260 °C. The hydrocarbon selectivities for the physical mixtures containing $NbOPO_4$ and γ-Al_2O_3 were around 2 $\%_C$ at the end of the experiment, however their increase throughout the experiment was markedly different. While the $NbOPO_4$-based catalyst showed a less pronounced increase in hydrocarbon selectivity after 20 h on stream, the γ-Al_2O_3-based catalyst showed a continuous increase throughout the experiment. The $Nb_2O_5{\cdot}nH_2O$-based mixture showed also at 280 °C the highest hydrocarbon selectivity. Hydrocarbon formation at 280 °C seemed to originate for all physical mixtures not only from the methanol synthesis catalysts but also from the addition of the solid acid.

The catalytic performance of the materials was further evaluated in a stacked-bed configuration, with the solid acid downstream of the methanol synthesis catalyst, this to further understand the synergy between the methanol synthesis catalyst and the solid acids. Table 3 summarizes the results for this experiment, the amount of solid acid was adjusted to have same amount of acid sites per reactor. Contrary to the physical mixtures, the CO conversion in this case was limited by the methanol synthesis catalyst and thus no major differences in conversion were observed within reactors (Fig. 3). Throughout the experiment, reactors with stacked-bed showed a decrease in activity similar to only the methanol synthesis catalyst at both reaction temperatures, implying that the activity loss originated mainly from the methanol synthesis catalyst and not the solid acids at these reaction conditions. CO_2 was not detected as a product since the copper-based catalyst was not exposed to the water formed from the dehydration of methanol and then the water-gas-shift reaction did not take place. However, addition of the solid acid downstream of the methanol synthesis catalyst changed the product distribution by forming DME at the expense of methanol. At both reaction temperatures, γ-Al_2O_3 showed the highest selectivity for DME, followed by $NbOPO_4$ and finally $Nb_2O_5{\cdot}nH_2O$. The differences in DME selectivity might be explained by the dissimilar densities and acid sites concentrations of each solid acid. Increasing the amount of $Nb_2O_5{\cdot}nH_2O$, the solid acid with the lowest concentration of acid sites per volume, indeed resulted in an increase in the DME selectivity (Table 3, second

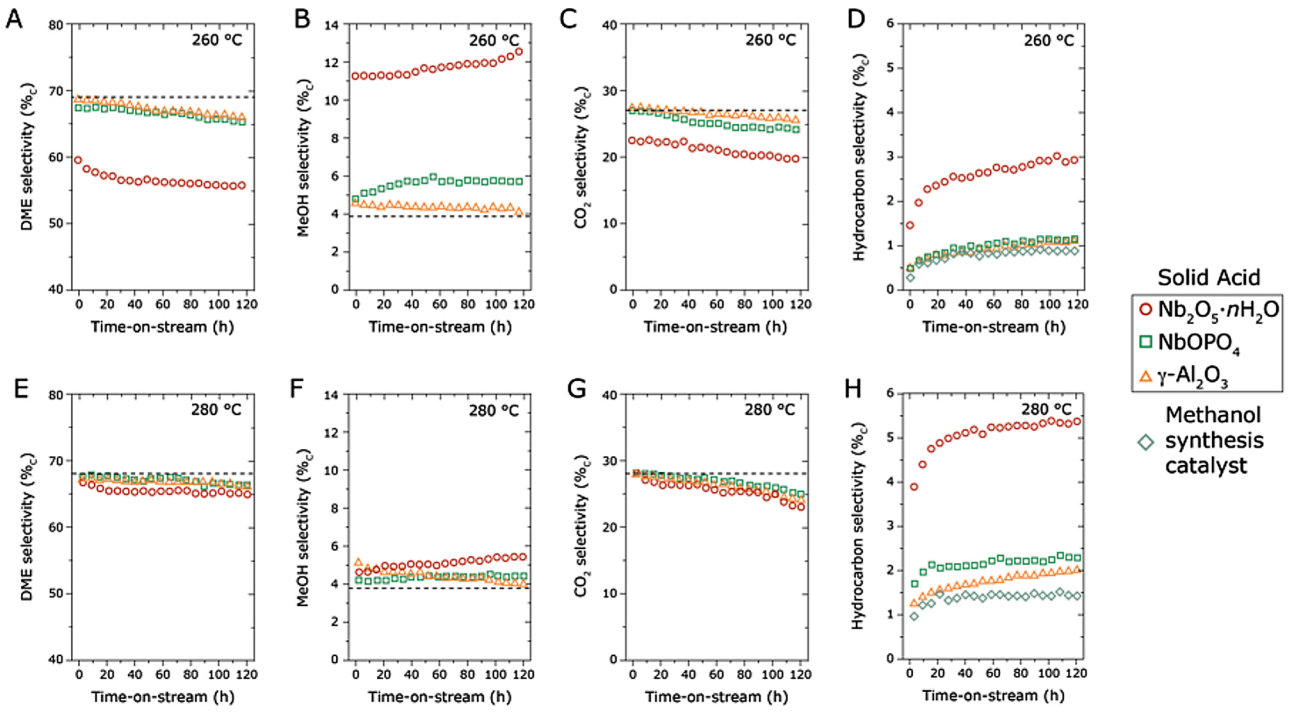

Fig. 4. Selectivities of the main products as a function of time-on-stream for the physical mixtures at 260 °C (A-D) or 280 °C (E-H): DME selectivity (A and E), methanol selectivity (B and F), CO_2 selectivity (C and G) and C_1 to C_4 hydrocarbon selectivity (D and H). The hydrocarbon selectivity for the methanol synthesis catalyst is also shown for comparison. Physical mixtures composed of 20 mg of copper-based methanol synthesis catalyst and ~ 0.2 mL of solid acid and the reaction conditions were 40 bar and $H_2/CO = 2$ v/v. Dashed lines indicate the corresponding thermodynamic equilibrium.

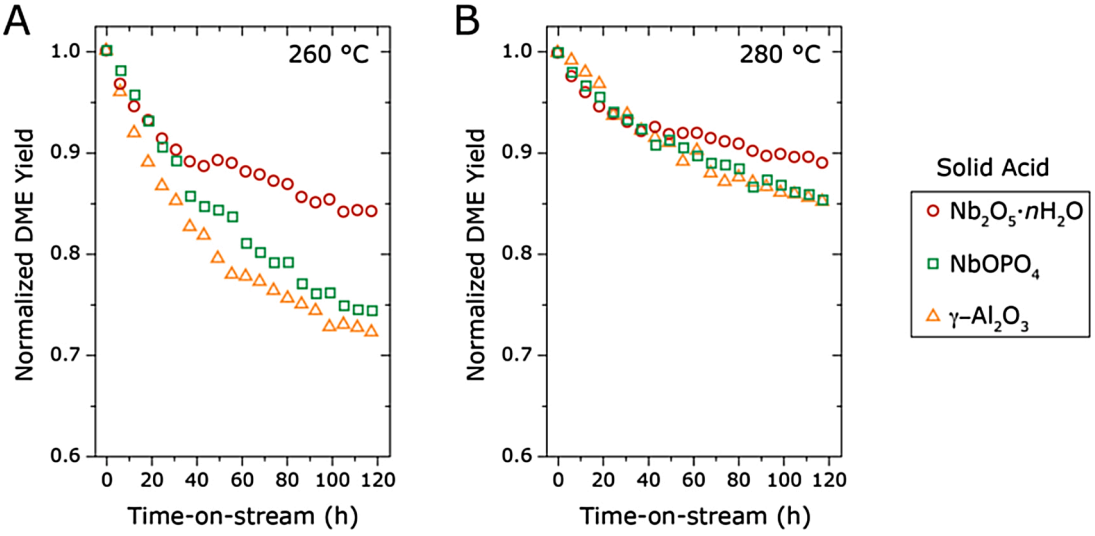

Fig. 5. Normalized DME yield as a function of time-on-stream at 260 °C (A) or 280 °C (B) for the physical mixtures composed of 20 mg of copper-based methanol synthesis catalyst and ~ 0.2 mL of solid acid. Reaction conditions: 40 bar, $H_2/CO = 2$ v/v and initial CO conversion between 61 and 71 % at 260 °C and between 79 and 82 % at 280 °C.

line). DME and methanol selectivities remained relatively constant throughout the experiment.

In contrast to the physical mixtures, the hydrocarbon selectivities of the reactors with solid acid and of only the methanol synthesis catalyst were similar throughout the experiment and increased to similar values by increasing reaction temperature (Fig. S5). The close contact of the methanol synthesis and dehydration functionalities in the physical mixtures, contrary to the stacked-bed configuration, could be then linked to the additional formation of hydrocarbons.

3.3. Characterization of the used catalysts

In order to further understand the reason behind deactivation in the physical mixtures, the used catalysts were separated by sieving them into the Cu-based methanol synthesis catalyst and the solid acid components. XRD patterns of the used solid acids (Fig. S6) did not show significant changes in comparison to the diffractograms of the materials before reaction. The niobium-based materials maintained an amorphous structure while the alumina remained in the gamma phase. Thus, a change in the crystal phase of the solid acid did not occur during the

Table 3
Summary of the reactor content and catalytic performance results in stacked-bed configuration, with the solid acid downstream of the methanol synthesis catalyst. Results of only the methanol synthesis catalysts are shown for comparison. Reaction conditions: 40 bar, $H_2/CO = 2$ v/v, 260 or 280 °C and TOS =120 h.

	Reactor content					Catalytic performance				
Reaction Temperature (°C)	Solid Acid	Mass of Methanol Synthesis Catalyst (upstream) (g)	Mass of Solid Acid (downstream) (g)	Total Amount acid sites[a] ($mmol_{NH3}$)	Total Volume (mL)	GHSV (h^{-1})	CO Conversion (%)	DME Selectivity ($\%_C$)	MeOH Selectivity ($\%_C$)	C_1-C_4 Hydrocarbon selectivity ($\%_C$)
260	$Nb_2O_5{\cdot}nH_2O$	0.015	0.020	0.0063	0.037	6000	9	41	58	1
		0.016	0.030	0.0093	0.049	4500	8	65	34	1
	$NbOPO_4$	0.016	0.010	0.0062	0.023	9600	8	52	47	1
	γ-Al_2O_3	0.015	0.010	0.0061	0.029	7700	9	81	19	1
	-	0.015	-	-	0.011	20100	9	0	99	1
280	$Nb_2O_5{\cdot}nH_2O$	0.010	0.011	0.0034	0.022	10000	8	59	39	2
	$NbOPO_4$	0.010	0.005	0.0030	0.014	16000	7	63	35	2
	γ-Al_2O_3	0.011	0.006	0.0037	0.019	12000	7	84	14	2
	-	0.010	-	-	0.008	28000	7	0	98	2

[a]Determined by NH_3-TPD.

reaction despite the high water partial pressures and the deactivation of the catalysts is not explained by this[38]. XRD characterization of their used Cu-based methanol synthesis catalyst showed growth of the Cu crystallite size in all cases (Fig. S7 and Table S1), particularly after the reaction at 280 °C. The actual crystallite size of the used catalysts might be slightly larger since these samples were passivated in air and part of the exposed copper most likely has been oxidized. Solely the Cu-based catalyst without solid acid after reaction showed a Cu crystallite size of 7.1 nm at 260 °C and of 7.6 nm at 280 °C compared to the reduced catalyst (6.6 nm). The Cu-based catalyst in the physical mixtures with the different solid acids displayed a larger crystallite growth compared to the catalyst without solid acid. However, the crystallite size variations within them could not be correlated to their deactivation trends.

Thus, only copper growth cannot explain the differences observed in loss of activity for the different physical mixtures. Besides metal growth, other structural changes aided by the presence of water could have taken place in the catalyst. Phenomena in the methanol synthesis catalyst such as re-crystallization of the ZnO or oxidation of the copper surface are relevant in the deactivation of the catalyst[67,68]. Here it was not possible to clearly observe such fine changes for all catalysts, only the Cu-based catalyst in the mixture with γ-Al_2O_3 after 280 °C reaction temperature (Fig. S7-J) showed a sharp diffraction peak at $2\theta = 40.7°$. This diffraction can correspond to the ZnO (002) reflection (PDF 00-003-0752), characteristic of ZnO nanowires[69,70]. Deterioration of the methanol synthesis catalyst during the reaction can then hamper the CO conversion and further DME formation.

The used solid acids were also characterized by thermogravimetric analysis in an oxidative atmosphere and monitored by MS in order to determine if deactivation might relate to coke deposition (Fig. S8). At temperatures below 200 °C the weight loss corresponded to the elimination of adsorbed water. Above 200 °C the weight loss was accompanied by the detection of CO_2 ($m/z = 44$, Fig. S8B and C), which most likely corresponded to burning of deposited coke. The change in weight was therefore normalized to the weight at 200 °C and weight loss was more pronounced for γ-Al_2O_3 (~ 4 $\%_w$), followed by $NbOPO_4$ (~ 2 $\%_w$) and $Nb_2O_5{\cdot}nH_2O$ (~ 1 $\%_w$). No marked difference in mass loss was observed when the catalysts had a reaction temperature at either 260 or 280 °C. Coke formation in solid acids can originate from accumulation

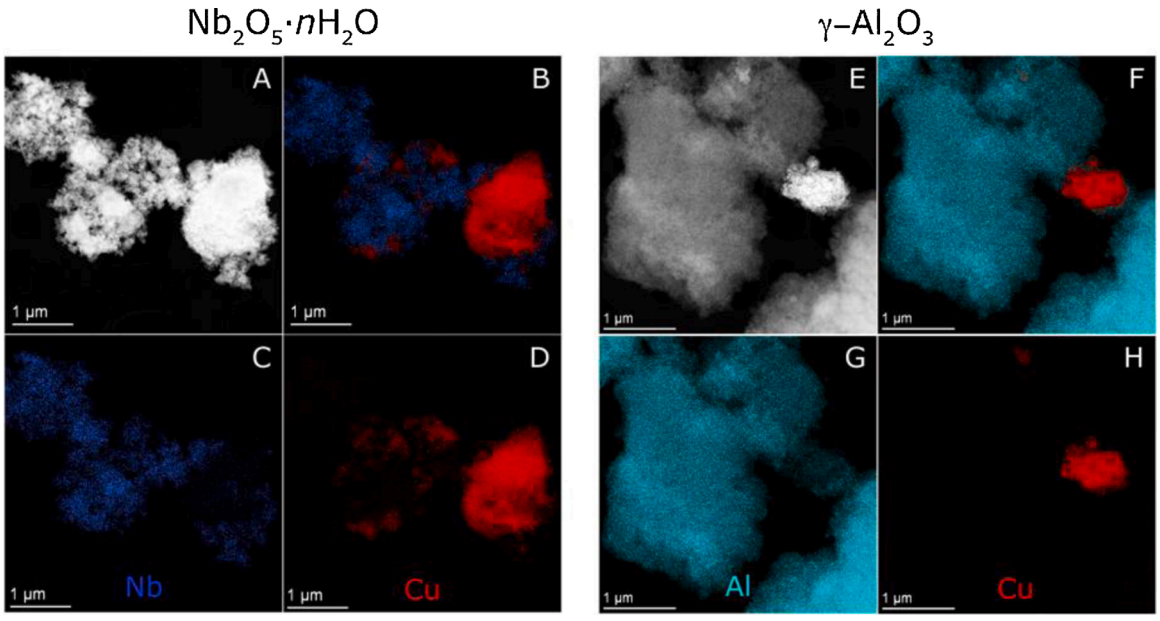

Fig. 6. STEM-EDX characterization results for the used mixtures of copper-based catalyst with $Nb_2O_5{\cdot}nH_2O$ (A-D) or γ-Al_2O_3 (E-H). A shows the dark-field image for the $Nb_2O_5{\cdot}nH_2O$-based mixture and B the overlap of the EDX-maps for Nb (blue) and Cu (red). The corresponding niobium and copper maps are shown in C and D respectively. E shows the dark-field image for the γ-Al_2O_3-based mixture and F the overlap of the EDX-maps for Al (light blue) and Cu (red). The corresponding aluminum and copper maps are shown in G and H respectively.

and side reactions of methoxy groups[71] (intermediate species for methanol dehydration) and even though weak acid sites typically show less tendency of coke formation[31], still constitutes a relevant source of deactivation[72,73].

Scanning transmission electron microscopy with energy dispersive X-ray spectra mapping (STEM-EDX) was used to characterize the used mixtures and the used solid acids after reaction at 260 °C. Fig. 6 shows the dark-field images and EDX elemental maps for the mixtures composed of the Cu-based catalyst and $Nb_2O_5{\cdot}nH_2O$ (left) or γ-Al_2O_3 (right). The EDX maps show the signal for Nb in dark blue, for Al in light blue and for Cu in red, Zn in all cases was found together with Cu so its EDX maps are not presented here for simplicity. In the case of $Nb_2O_5{\cdot}nH_2O$ is possible to observe that Nb and Cu in some areas are very close together and even showing some overlap. On the left side of the EDX maps it seems that Cu is dispersed on the niobium oxide and on the right side the big copper particle seems to be covered with some niobium oxide. For γ-Al_2O_3, the areas corresponding to Al and Cu are also close together but they seem to be more localized, is possible to observe an overlap in the particle on the right side of the Cu with Al because the methanol synthesis catalyst also contains alumina, however the big particles with Al which correspond to γ-Al_2O_3 do not show an overlap with the Cu signal. It has been previously shown that migration of ions in bifunctional systems occurs, leading to a deterioration of the catalytic performance with time[4]. The overlap in Cu and Nb signal might be an indication that metals from the methanol synthesis catalyst might have migrated to the $Nb_2O_5{\cdot}nH_2O$ during the reaction, compromising the performance of both the methanol synthesis catalyst and the solid acid. Moreover, this close contact of the copper and acid functionality might have had a relationship with the increased hydrocarbon selectivity of the physical mixtures via methoxy migration and decomposition[74,75]. The differences in hydrocarbon selectivities within solid acids might relate to the extent of copper migration to the solid acid.

EDX maps of only the used solid acids (Fig. S9) showed a uniform overlap of Cu and Nb for $NbOPO_4$ and $Nb_2O_5{\cdot}nH_2O$, an indication that the copper might be homogenously distributed over the surface of these solid acids after reaction. The Cu-Kα signal of the corresponding spectra was more intense for $NbOPO_4$ than for $Nb_2O_5{\cdot}nH_2O$ or γ-Al_2O_3. Furthermore, the niobium-based materials had a green grayish color after reaction, an indication of a copper compound on their surface, whereas the alumina remained white. Migration of copper to the surface of the niobium-based materials could have been aided by the presence of Brønsted acid sites, which alumina did not show, via an ion exchange aided transport. Further research into the exact mechanism is needed to thoroughly understand the phenomenon.

4. Conclusions

In this study we investigated the catalytic performance of hydrated niobium pentoxide and niobium phosphate as solid acids combined with a copper-based methanol synthesis catalyst for the direct synthesis of DME from synthesis gas. Gamma-alumina, a commonly used solid acid for this reaction, was investigated as a reference material. The solid acids were physically mixed with the copper-based methanol synthesis catalyst and their catalytic performance was evaluated at 40 bar, H_2/CO = 2 v/v and two different reaction temperatures (260 or 280 °C) for 120 h on stream. The mixing of the methanol synthesis catalyst and the solid acid led to increased CO conversions, compared to the methanol synthesis catalyst without solid acid or arranged in stacked-bed configuration with the solid acid downstream of the methanol synthesis catalyst. All physical mixtures showed excellent activity and DME selectivity. Particularly, niobium phosphate performed as good as gamma-alumina, with improved DME productivity per unit volume due to its high density and acid site concentration. However, the close contact between both functionalities in all mixtures also led to a slight increase in C_1-C_4 hydrocarbon selectivities. Furthermore, the stabilities of all mixtures differed depending on the nature of the solid acid, indicative of different deactivation mechanisms. The used catalysts were characterized in order to understand the main cause of deactivation. XRD results showed that the solid acids maintained their initial crystal structures after the reaction, therefore a major structural rearrangement in the solid acids was not the cause of deactivation under the reaction conditions used here. Cu crystallite size of the methanol synthesis catalyst grew during reaction conditions, but their growth was similar within the different mixtures so deactivation could not be solely explained by the loss of copper surface area. However, other structural changes in the Cu-based catalyst could not be completely excluded, one of the Cu-based catalysts in a mixture with γ-Al_2O_3 after reaction showed an extra diffraction peak corresponding to ZnO nanostructure, an indication that the methanol catalyst could be susceptible to structural changes during DME synthesis. Thermogravimetric analysis of the used solid acids showed that γ-Al_2O_3 accumulated more coke compared to the niobium-based materials, which might partially explain the loss in DME production particularly for γ-Al_2O_3. EDX analysis of STEM images of the used catalysts revealed that the niobium-based solid acids and not the alumina one ended up with some copper on their surface after reaction. This might be an indication of ion migration from the copper-based methanol synthesis catalyst to the surface of the solid acids, and most likely compromising the performance of both the methanol synthesis catalyst and the acid sites. $Nb_2O_5{\cdot}nH_2O$ and $NbOPO_4$ showed Lewis and Brønsted acid sites, while γ-Al_2O_3 showed only Lewis acid sites, this might explain the susceptibility of Cu migration in the case of the niobium-based materials. To summarize, the catalytic performance and characterization results point out that deactivation of the physical mixtures originated mainly from structural changes in the methanol synthesis catalysts. In the case of $Nb_2O_5{\cdot}nH_2O$ and $NbOPO_4$, the deactivation might relate mainly to the migration of copper from the methanol synthesis catalyst to the Brønsted acid sites of these materials, while in the case of γ-Al_2O_3 deactivation might have generated from crystallite reconstruction of the ZnO in the methanol synthesis catalyst and coke deposition on the acid sites.

CRediT authorship contribution statement

C. Hernández Mejía: Conceptualization, Methodology, Investigation, Writing - original draft. **D.M.A. Verbart:** Methodology, Investigation. **K.P. de Jong:** Conceptualization, Writing - review & editing, Supervision.

Declaration of Competing Interest

The authors declare that they have no known competing financial interests or personal relationships that could have appeared to influence the work reported in this paper.

Acknowledgements

Companhia Brasileira de Metalurgia e Mineração (CBMM) is thanked for financial support of this research. Dr. Robson Monteiro and Mr. Rogério Ribas (CBMM) are acknowledged for useful discussions and supplying the niobium-based materials. Mrs. Savannah Turner and Mr. Dennie Wezendonk (Utrecht University) are acknowledged for performing STEM-EDX and TGA-MS measurements respectively. Mr. Miguel Rivera-Torrente (Utrecht University) is acknowledged for his help during the FTIR measurements. Dr. Kang Cheng (Utrecht University) is thanked for useful thermodynamic discussions. Mr. Lennart Weber, Mr. Rolf Beerthuis and Mr. Remco Dalebout are thanked for their support during the catalytic performance and maintenance of the Flowrence unit. Krijn P. de Jong acknowledges the European Research Council, EU FP7 ERC Advanced Grant no. 338846.

Appendix A. Supplementary data

Supplementary material related to this article can be found, in the online version, at doi:https://doi.org/10.1016/j.cattod.2020.07.059.

References

[1] W. Zhou, K. Cheng, J. Kang, C. Zhou, V. Subramanian, Q. Zhang, Y. Wang, New horizon in C1 chemistry: Breaking the selectivity limitation in transformation of syngas and hydrogenation of CO2 into hydrocarbon chemicals and fuels, Chem. Soc. Rev. 48 (2019) 3193–3228, https://doi.org/10.1039/c8cs00502h.

[2] J. Bao, G. Yang, Y. Yoneyama, N. Tsubaki, Significant advances in C1 catalysis: highly efficient catalysts and catalytic reactions, ACS Catal. 9 (2019) 3026–3053, https://doi.org/10.1021/acscatal.8b03924.

[3] J. Zecevic, G. Vanbutsele, K.P. De Jong, J.A. Martens, Nanoscale intimacy in bifunctional catalysts for selective conversion of hydrocarbons, Nature. 528 (2015) 245–254, https://doi.org/10.1038/nature16173.

[4] J.L. Weber, N.A. Krans, J.P. Hofmann, E.J.M. Hensen, J. Zecevic, P.E. de Jongh, K. P. de Jong, Effect of proximity and support material on deactivation of bifunctional catalysts for the conversion of synthesis gas to olefins and aromatics, Catal. Today. (2019) 1–6, https://doi.org/10.1016/j.cattod.2019.02.002.

[5] H. Ham, J. Kim, S.J. Cho, J.H. Choi, D.J. Moon, J.W. Bae, Enhanced Stability of Spatially Confined Copper Nanoparticles in an Ordered Mesoporous Alumina for Dimethyl Ether Synthesis from Syngas, ACS Catal. 6 (2016) 5629–5640, https://doi.org/10.1021/acscatal.6b00882.

[6] C. Jeong, H. Ham, J.W. Bae, D. Kang, C. Shin, J.H. Baik, Y. Suh, Facile Structure Tuning of a Methanol-Synthesis Catalyst towards the Direct Synthesis of Dimethyl Ether from Syngas, ChemCatChem. 9 (2017) 4484–4489, https://doi.org/10.1002/cctc.201701167.

[7] J.L. Weber, I. Dugulan, P.E. de Jongh, K.P. de Jong, Bifunctional Catalysis for the Conversion of Synthesis Gas to Olefins and Aromatics, ChemCatChem. 10 (2018) 1107–1112, https://doi.org/10.1002/cctc.201701667.

[8] M. Müller, U. Hübsch, Dimethyl Ether, Ullmann's Encycl, Ind. Chem. (2012), https://doi.org/10.1002/14356007.a08.

[9] A.W. Budiman, J.S. Nam, J.H. Park, R.I. Mukti, T.S. Chang, J.W. Bae, M.J. Choi, Review of Acetic Acid Synthesis from Various Feedstocks Through Different Catalytic Processes, Catal. Surv. from Asia. 20 (2016) 173–193, https://doi.org/10.1007/s10563-016-9215-9.

[10] W. Song, D.M. Marcus, H. Fu, J.O. Ehresmann, J.F. Haw, An Oft-Studied Reaction That May Never Have Been: Direct Catalytic Conversion of Methanol or Dimethyl Ether to Hydrocarbons on the Solid Acids HZSM-5 or HSAPO-34, J. Am. Chem. Soc. 124 (2002) 3844–3845, https://doi.org/10.1021/ja016499u.

[11] F. Joensen, B. Voss, I. Dybkjaer, Process for the preparation of acetic acid, 5728871, 1998.

[12] R.P. Verbeek, A. van Doorn, M. van Walwijk, Global assessment of Dimethyl-ether as an automotive fuel, 1996.

[13] T.A. Semelsberger, R.L. Borup, H.L. Greene, Dimethyl ether (DME) as an alternative fuel, J. Power Sources. 156 (2006) 497–511, https://doi.org/10.1016/j.jpowsour.2005.05.082.

[14] T.H. Fleisch, A. Basu, R.A. Sills, Introduction and advancement of a new clean global fuel: The status of DME developments in China and beyond, J. Nat. Gas Sci. Eng. 9 (2012) 94–107, https://doi.org/10.1016/j.jngse.2012.05.012.

[15] I. Dybkjær, J.B. Hansen, Large-scale production of alternative synthetic fuels from natural gas, Stud. Surf. Sci. Catal. 107 (1997) 99–116, https://doi.org/10.1016/s0167-2991(97)80322-9.

[16] T. Ogawa, N. Inoue, T. Shikada, Y. Ohno, Direct Dimethyl Ether Synthesis, J. Nat. Gas Chem. 12 (2003) 219–227.

[17] J. Topp-Jørgensen, Topsøe Integrated Gasoline Synthesis – The Tigas Process, Stud. Surf. Sci. Catal. 36 (1988) 293–305, https://doi.org/10.1016/S0167-2991(09)60523-1.

[18] M. Behrens, Promoting the Synthesis of Methanol: Understanding the Requirements for an Industrial Catalyst for the Conversion of CO 2, Angew. Chemie Int. Ed. 55 (2016) 14906–14908, https://doi.org/10.1002/anie.201607600.

[19] F. Dadgar, R. Myrstad, P. Pfeifer, A. Holmen, H.J. Venvik, Direct dimethyl ether synthesis from synthesis gas: The influence of methanol dehydration on methanol synthesis reaction, Catal. Today. 270 (2016) 76–84, https://doi.org/10.1016/j.cattod.2015.09.024.

[20] C.H. Bartholomew, Mechanisms of catalyst deactivation, Appl. Catal. A Gen. 212 (2001) 17–60, https://doi.org/10.1016/S0926-860X(00)00843-7.

[21] J. Sun, G. Yang, Y. Yoneyama, N. Tsubaki, Catalysis chemistry of dimethyl ether synthesis, ACS Catal. 4 (2014) 3346–3356, https://doi.org/10.1021/cs500967j.

[22] Z. Azizi, M. Rezaeimanesh, T. Tohidian, M.R. Rahimpour, Dimethyl ether: A review of technologies and production challenges, Chem. Eng. Process. Process Intensif. 82 (2014) 150–172, https://doi.org/10.1016/j.cep.2014.06.007.

[23] J. Sehested, Industrial and scientific directions of methanol catalyst development, J. Catal. 371 (2019) 368–375, https://doi.org/10.1016/j.jcat.2019.02.002.

[24] K.C. Waugh, Methanol Synthesis, Catal. Today. 15 (1992) 51–75, https://doi.org/10.1016/0920-5861(92)80122-80124.

[25] D. Sheldon, Methanol production - A technical history, Johnson Matthey Technol, Rev. 61 (2017) 172–182, https://doi.org/10.1595/205651317X695622.

[26] G.A. Olah, A. Goeppert, G.K.S. Prakash, Chemical recycling of carbon dioxide to methanol and dimethyl ether: From greenhouse gas to renewable, environmentally carbon neutral fuels and synthetic hydrocarbons, J. Org. Chem. 74 (2009) 487–498, https://doi.org/10.1021/jo801260f.

[27] A. Álvarez, A. Bansode, A. Urakawa, A.V. Bavykina, T.A. Wezendonk, M. Makkee, J. Gascon, F. Kapteijn, Challenges in the Greener Production of Formates/Formic Acid, Methanol, and DME by Heterogeneously Catalyzed CO2 Hydrogenation Processes, Chem. Rev. 117 (2017) 9804–9838, https://doi.org/10.1021/acs.chemrev.6b00816.

[28] S.R. Blaszkowski, R.A. Van Santen, The mechanism of dimethyl ether formation from methanol catalyzed by zeolitic protons, J. Am. Chem. Soc. 118 (1996) 5152–5153, https://doi.org/10.1021/ja954323k.

[29] H. Knözinger, R. Köhne, The dehydration of alcohols over alumina. I. The reaction scheme, J. Catal. 5 (1966) 264–270, https://doi.org/10.1016/S0021-9517(66)80007-6.

[30] J.J. Spivey, Review: Dehydration catalysts for the methanol/dimethyl ether reaction, Chem. Eng. Commun. 110 (1991) 123–142, https://doi.org/10.1080/00986449108939946.

[31] S. Tamm, Coking During DME Synthesis: A Calorimeter Study, Top. Catal. 58 (2015) 833–842, https://doi.org/10.1007/s11244-015-0450-5.

[32] Y. Wei, P.E. De Jongh, M.L.M. Bonati, D.J. Law, G.J. Sunley, K.P. De Jong, Enhanced catalytic performance of zeolite ZSM-5 for conversion of methanol to dimethyl ether by combining alkaline treatment and partial activation, Appl. Catal. A Gen. 504 (2015) 211–219, https://doi.org/10.1016/j.apcata.2014.12.027.

[33] V. Vishwanathan, K.W. Jun, J.W. Kim, H.S. Roh, Vapour phase dehydration of crude methanol to dimethyl ether over Na-modified H-ZSM-5 catalysts, Appl. Catal. A Gen. 276 (2004) 251–255, https://doi.org/10.1016/j.apcata.2004.08.011.

[34] I. Štich, J.D. Gale, K. Terakura, M.C. Payne, Role of the zeolitic environment in catalytic activation of methanol, J. Am. Chem. Soc. 121 (1999) 3292–3302, https://doi.org/10.1021/ja983470q.

[35] M. Xu, J.H. Lunsford, D.W. Goodman, A. Bhattacharyya, Synthesis of dimethyl ether (DME) from methanol over solid-acid catalysts, Appl. Catal. A Gen. 149 (1997) 289–301, https://doi.org/10.1016/S0926-860X(96)00275-X.

[36] H. Topsøe, DME-99 ECO^{TM}, 2019. https://www.topsoe.com/products/catalysts/dme-99-ecotm.

[37] J. Boon, J. van Kampen, R. Hoogendoorn, S. Tanase, F.P.F. van Berkel, M. van Sint Annaland, Reversible deactivation of γ-alumina by steam in the gas-phase dehydration of methanol to dimethyl ether, Catal. Commun. 119 (2019) 22–27, https://doi.org/10.1016/j.catcom.2018.10.008.

[38] S.S. Akarmazyan, P. Panagiotopoulou, A. Kambolis, C. Papadopoulou, D. I. Kondarides, Methanol dehydration to dimethylether over Al2O3 catalysts, Appl. Catal. B Environ. 145 (2014) 136–148, https://doi.org/10.1016/j.apcatb.2012.11.043.

[39] I. Nowak, M. Ziolek, Niobium Compounds: Preparation, Characterization, and Application in Heterogeneous Catalysis, Chem. Rev. 99 (1999) 3603–3624, https://doi.org/10.1021/cr9800208.

[40] K. Tanabe, Catalytic application of niobium compounds, Catal. Today. 78 (2003) 65–77, https://doi.org/10.1016/S0920-5861(02)00343-7.

[41] S. Okazaki, N. Wada, Surface properties and catalytic activities of amorphous niobium phosphate and a comparison with those of H3PO4-treated niobium oxide, Catal. Today. 16 (1993) 349–359, https://doi.org/10.1016/0920-5861(93)80074-B.

[42] S. Hayashi, M. Hara, K. Nakajima, Y. Baba, R. Noma, M. Kitano, J.N. Kondo, S. Hayashi, M. Hara, $Nb_2O_5.nH_2O$ as a Heterogeneous Catalyst with Water-Tolerant Lewis Acid Sites, J. Am. Chem. Soc. 133 (2011) 4224–4227, https://doi.org/10.1016/j.ijleo.2015.05.036.

[43] T. Ushikubo, Y. Koike, K. Wada, L. Xei, D. Wang, X. Guo, Study of the structure of niobium oxide by X-ray absorption fine structure and surface science techniques, Catal. Today. 28 (1996) 59–69, https://doi.org/10.1016/0920-5861(95)00230-8.

[44] P. Carniti, A. Gervasini, F. Bossola, V. Dal Santo, Cooperative action of Brønsted and Lewis acid sites of niobium phosphate catalysts for cellobiose conversion in water, Appl. Catal. B Environ. 193 (2016) 93–102, https://doi.org/10.1016/j.apcatb.2016.04.012.

[45] Q. Sun, Y. Fu, H. Yang, A. Auroux, J. Shen, Dehydration of methanol to dimethyl ether over Nb2O5and NbOPO4catalysts: Microcalorimetric and FT-IR studies, J. Mol. Catal. A Chem. 275 (2007) 183–193, https://doi.org/10.1016/j.molcata.2007.06.008.

[46] D. Liu, C. Yao, J. Zhang, D. Fang, D. Chen, Catalytic dehydration of methanol to dimethyl ether over modified γ-Al2O3catalyst, Fuel. 90 (2011) 1738–1742, https://doi.org/10.1016/j.fuel.2011.01.038.

[47] R. Ladera, E. Finocchio, S. Rojas, J.L.G. Fierro, M. Ojeda, Supported niobium catalysts for methanol dehydration to dimethyl ether: FTIR studies of acid properties, Catal. Today. 192 (2012) 136–143, https://doi.org/10.1016/j.cattod.2012.01.025.

[48] A.S. Rocha, A.M. Aline, E.R. Lachter, E.F. Sousa-Aguiar, A.C. Faro, Niobia-modified aluminas prepared by impregnation with niobium peroxo complexes for dimethyl ether production, Catal. Today. 192 (2012) 104–111, https://doi.org/10.1016/j.cattod.2012.02.062.

[49] S.H. Lima, A.M.S. Forrester, L.A. Palacio, A.C. Faro, Niobia-alumina as methanol dehydration component in mixed catalyst systems for dimethyl ether production from syngas, Appl. Catal. A Gen. 488 (2014) 19–27, https://doi.org/10.1016/j.apcata.2014.09.022.

[50] M. Wojdyr, Fityk: A general-purpose peak fitting program, J. Appl. Crystallogr. 43 (2010) 1126–1128, https://doi.org/10.1107/S0021889810030499.

[51] C.A. Emeis, Determination of integrated molar extinction coefficients for infrared absorption bands of pyridine adsorbed on solid acid catalysts, J. Catal. 141 (1993) 347–354, https://doi.org/10.1006/jcat.1993.1145.

[52] H. Schäfer, R. Gruehn, F. Schulte, The Modifications of Niobium Pentoxide, Angew. Chemie Int. Ed. English. 5 (1966) 40–52, https://doi.org/10.1002/anie.196600401.

[53] K.J. Griffith, A.C. Forse, J.M. Griffin, C.P. Grey, High-Rate Intercalation without Nanostructuring in Metastable Nb2O5 Bronze Phases, J. Am. Chem. Soc. 138 (2016) 8888–8899, https://doi.org/10.1021/jacs.6b04345.
[54] T. Iizuka, K. Ogasawara, K. Tanabe, Acidic and catalytic properties of niobium pentaoxide, Bull. Chem. Soc. Jpn. 56 (1983) 2927–2931, https://doi.org/10.1246/bcsj.56.2927.
[55] C. Hernández Mejía, J.H. den Otter, J.L. Weber, K.P. de Jong, Crystalline niobia with tailored porosity as support for cobalt catalysts for the Fischer–Tropsch synthesis, Appl. Catal. A Gen. 548 (2017) 143–149, https://doi.org/10.1016/j.apcata.2017.07.016.
[56] V. Lebarbier, M. Houalla, T. Onfroy, New insights into the development of Bronsted acidity of niobic acid, Catal. Today. 192 (2012) 123–129, https://doi.org/10.1016/j.cattod.2012.02.061.
[57] A. Florentino, P. Cartraud, P. Magnoux, M. Guisnet, Textural, acidic and catalytic properties of niobium phosphate and of niobium oxide. Influence of the pretreatment temperature, Appl. Catal. A, Gen. 89 (1992) 143–153, https://doi.org/10.1016/0926-860X(92)80229-6.
[58] C.H. Kline, J. Turkevich, The vibrational spectrum of pyridine and the thermodynamic properties of pyridine vapors, J. Chem. Phys. 12 (1944) 300–309, https://doi.org/10.1063/1.1723943.
[59] C. Morterra, G. Magnacca, A case study: Surface chemistry and surface structure of catalytic aluminas, as studied by vibrational spectroscopy of adsorbed species, Catal. Today. 27 (1996) 497–532, https://doi.org/10.1016/0920-5861(95)00163-8.
[60] E.P. Parry, An infrared study of pyridine adsorbed on acidic solids. Characterization of surface acidity, J. Catal. 2 (1963) 371–379, https://doi.org/10.1016/0021-9517(63)90102-7.
[61] X. Liu, R.E. Truitt, DRFT-IR studies of the surface of γ-Alumina, J. Am. Chem. Soc. 119 (1997) 9856–9860, https://doi.org/10.1021/ja971214s.
[62] J. Datka, A.M. Turek, J.M. Jehng, I.E. Wachs, Acidic properties of supported niobium oxide catalysts: An infrared spectroscopy investigation, J. Catal. 135 (1992) 186–199, https://doi.org/10.1016/0021-9517(92)90279-Q.
[63] R.T. Carr, M. Neurock, E. Iglesia, Catalytic consequences of acid strength in the conversion of methanol to dimethyl ether, J. Catal. 278 (2011) 78–93, https://doi.org/10.1016/j.jcat.2010.11.017.
[64] S.R. Blaszkowski, R.A. Van Santen, The mechanism of dimethyl ether formation from methanol catalyzed by zeolitic protons, J. Am. Chem. Soc. 118 (1996) 5152–5153, https://doi.org/10.1021/ja954323k.
[65] G.S. Foo, D. Wei, D.S. Sholl, C. Sievers, Role of Lewis and brønsted acid sites in the dehydration of glycerol over niobia, ACS Catal. 4 (2014) 3180–3192, https://doi.org/10.1021/cs5006376.
[66] R. Peláez, E. Bryce, P. Marín, S. Ordóñez, Catalyst deactivation in the direct synthesis of dimethyl ether from syngas over CuO/ZnO/Al2O3 and Γ-Al2O3 mechanical mixtures, Fuel Process. Technol. 179 (2018) 378–386, https://doi.org/10.1016/j.fuproc.2018.07.029.
[67] T. Lunkenbein, F. Girgsdies, T. Kandemir, N. Thomas, M. Behrens, R. Schlögl, E. Frei, Bridging the Time Gap: A Copper/Zinc Oxide/Aluminum Oxide Catalyst for Methanol Synthesis Studied under Industrially Relevant Conditions and Time Scales, Angew. Chemie - Int. Ed. 55 (2016) 12708–12712, https://doi.org/10.1002/anie.201603368.
[68] B. Liang, J. Ma, X. Su, C. Yang, H. Duan, H. Zhou, S. Deng, L. Li, Y. Huang, Investigation on Deactivation of Cu/ZnO/Al2O3 Catalyst for CO2 Hydrogenation to Methanol, Ind. Eng. Chem. Res. 58 (2019) 9030–9037, https://doi.org/10.1021/acs.iecr.9b01546.
[69] M. Laurenti, V. Cauda, R. Gazia, M. Fontana, V.F. Rivera, S. Bianco, G. Canavese, Wettability control on ZnO nanowires driven by seed layer properties, Eur. J. Inorg. Chem. 2013 (2013) 2520–2527, https://doi.org/10.1002/ejic.201201420.
[70] Y. Tak, K. Yong, Controlled growth of well-aligned ZnO nanorod array using a novel solution method, J. Phys. Chem. B. 109 (2005) 19263–19269, https://doi.org/10.1021/jp0538767.
[71] H. Yamazaki, H. Shima, H. Imai, T. Yokoi, T. Tatsumi, J.N. Kondo, Direct production of propene from methoxy species and dimethyl ether over H-ZSM-5, J. Phys. Chem. C. 116 (2012) 23851–24392, https://doi.org/10.1021/jp307290z.
[72] J. Ereña, I. Sierra, M. Olazar, A.G. Gayubo, A.T. Aguayo, Deactivation of a CuO-ZnO-Al2O3/γ-Al2O3 catalyst in the synthesis of dimethyl ether, Ind. Eng. Chem. Res. 47 (2008) 2238–2247, https://doi.org/10.1021/ie071478f.
[73] I. Sierra, J. Ereña, A.T. Aguayo, M. Olazar, J. Bilbao, Deactivation kinetics for direct dimethyl ether synthesis on a CuO-ZnO-Al2O3/γ-Al2O3 Catalyst, Ind. Eng. Chem. Res. 49 (2010) 481–489, https://doi.org/10.1021/ie900978a.
[74] B. Sen, J.L. Falconer, T.F. Mao, M. Yu, R.L. Flesner, Spillover of CO and H2 onto Al2O3 surfaces, J. Catal. 126 (1990) 465–476, https://doi.org/10.1016/0021-9517(90)90013-A.
[75] B. Chen, J.L. Falconer, Hydrogenation of organic oxygenates on Ni/Al2O3 and Ni/SiO2 catalysts, J. Catal. 147 (1994) 72–81, https://doi.org/10.1006/jcat.1994.1115.